

Eigenanalysis of silicon random nanostructures formed via resist collapse for nano-artifact metrics

**Makoto Naruse^{1*}, Morihisa Hoga², Yasuyuki Ohyagi², Shumpei Nishio²,
Naoya Tate³, Naoki Yoshida⁴, and Tsutomu Matsumoto^{4,5}**

*¹Photonic Network Research Institute, National Institute of Information and Communications
Technology, 4-2-1 Nukui-kita, Koganei, Tokyo 184-8795, Japan*

²Dai Nippon Printing Co. Ltd., 250-1 Wakashiba, Kashiwa, Chiba 277-0871, Japan

*³ Graduate School of Information Science and Electrical Engineering, Kyushu University, 744
Motooka, Nishi-ku, Fukuoka 819-0395, Japan*

*⁴ Graduate School of Environment and Information Sciences, Yokohama National University,
79-7 Tokiwadai, Hodogaya, Yokohama 240-8501, Japan*

*⁵ Institute of Advanced Sciences, Yokohama National University, 79-5 Tokiwadai, Hodogaya,
Yokohama 240-8501, Japan*

* E-mail: naruse@nict.go.jp

ABSTRACT: With an eigenanalysis approach, this paper quantitatively unveils the diversity and the capacity of identities offered by silicon random nanostructures formed via random collapse of resist for nano-artifact metrics or physical unclonable functions, which are vital in the Internet-of-Things era where securing the identity of individual devices is critical. The results provide about 10^{115} possible identities per $0.18\text{-}\mu\text{m}^2$ area of nanostructures, indicating that nanoscale versatile morphology will be extremely useful for future security functions. Also, the result validates the effectiveness and the usefulness of eigenanalysis approaches for versatile nanostructures, which will be widely applicable to other nanomaterials and morphological patterns.

Artifact metrics,¹ also called physical unclonable function (PUF),² use the unique physical properties of individual objects. These include electromagnetic,³ mechanical, and optical properties⁴ associated with the objects such as ordinary paper,⁵ paper containing magnetic microfibers,⁶ plastics, and semiconductor chips. The concept of *nano-artifact metrics* was proposed and experimentally demonstrated by Matsumoto *et al.*⁷ In order to protect against cloning attacks, nano-artifact metrics exploit the physically uncontrollable processes occurring at the nanometer-scale, which are beyond the scope of nanostructure technologies.

In particular, nano-artifact metrics utilize the random collapse of resists induced by exposure to electron-beam (e-beam) lithography.⁷ Resist collapse may occur during the rinse process of lithography, and depends on the pattern resolution, resist thickness, and duration of e-beam exposure.⁸ The result is the collapse of the intended pattern, whose minimum dimensions are smaller than the resolutions of nanofabrication technologies.⁷ The basic performance for security applications was clarified in Ref. 7 by quantitatively evaluating the false-match rate for verifying identities, the false non-match rate (FNMR) for characterizing the stability of measurements, and the clone-match rate for evaluating the difficulties in making clones.

However, the technology's potential is not completely known yet, especially in terms of the number of different devices or identities that could be distinguished based on the nanoscale morphological characteristics. This is especially important in view of future applications such as document security,⁹ Internet-of-Things (IoT),¹⁰ and others. In this study, we perform eigenanalysis of experimentally fabricated silicon random nanostructures, through which the diversity and the potential capacity of identities are quantitatively estimated.

First, we review the experimental devices used for our nano-artifact metrics. We fabricated an array of resist pillars with a $60\text{ nm} \times 60\text{ nm} \times 200\text{ nm}$ cross-sectional area on a

grid of $120 \text{ nm} \times 120 \text{ nm}$ squares that filled a $2 \text{ }\mu\text{m} \times 2 \text{ }\mu\text{m}$ square, as shown in Fig. 1(a). We used an e-beam lithography system (JEOL JBX-9300FS) with a 100-kV acceleration voltage. In the rinse process, the random collapse of resist pillars was induced as shown in the scanning electron microscope (SEM) image in Fig. 1(b). The resulting patterns were imaged by a critical-dimension SEM (CD-SEM, Hitachi High-Technologies CG4000). We analyzed 2383 samples fabricated on a single 200-mm-diameter wafer. Figures 1(c) and (d) show examples of SEM images of an array of collapsed resist pillars. The image contains 1024×1024 pixels and has an 8-bit resolution (256 levels). Versatile morphologies were observed, and the structural detail of the patterns (Fig. 1(c)) is as small as 9.23 nm.⁷

We conducted the following eigenanalysis. An 8-bit (256 levels) greyscale image of size 128×128 pixels was extracted from around the center of a pillar array image and smoothed using an 11×11 median filter. Here, one pixel occupies approximately a 3.3 nm square area; therefore, the area of a single image is about $0.18 \text{ }\mu\text{m}^2$. We denote an image by a vector \mathbf{x}_i , which has $P = 128 \times 128$ elements. All the images or the total sets of nano-artifact metrics devices are summarized by a matrix

$$Z = \{\mathbf{x}_1, \mathbf{x}_2, \dots, \mathbf{x}_N\}, \quad (1)$$

where N is the number of devices, which is 2383 in the present study. Let the mean values of all images be given by

$$\boldsymbol{\mu} = \frac{1}{N} \sum_{i=1}^N \mathbf{x}_i. \quad (2)$$

The covariance matrix is given by

$$C = \frac{1}{N} (Z - \boldsymbol{\mu})^T (Z - \boldsymbol{\mu}), \quad (3)$$

where T indicates the matrix transpose and $(Z - \mu)$ implies subtracting the vector μ from each column of matrix Z . By solving the eigenequation

$$C\mathbf{s}_k = \lambda_k \mathbf{s}_k, \quad (4)$$

we derive the eigenvalues λ_k and the eigenvectors \mathbf{s}_k . We set the index k so that the eigenvalues are arranged in descending order. Such an eigen decomposition approach in analyzing a cluster of images is widely used in image processing literature¹¹ as well as in other high-dimensional systems such as robotic manipulators¹² and alignment of optical systems¹³.

Figure 2(a) shows the cumulative sum of the eigenvalues divided by their sum. From this evaluation, 98% of the original images cannot be retrieved if we do not consider eigenvectors up to the 424th order, indicating that the image space or the nano-artifact metric device spans a vast volume of high-dimensional eigenspaces (inset of Fig. 2(a)). Figure 2(b) shows the eigenvectors corresponding to the eigenvalues [from the 1st to the 10th], [from the 30th to the 39th], and [from the 400th to the 409th], each represented by a two-dimensional image. The eigenvectors with eigenvalues around the 400th order contain single-pixel-level resolution and fine-scale structures. Our interest is to reveal the potential and the limitation of the approaches utilizing such morphological characters quantitatively.

Each image or nano-artifact metrics device \mathbf{x}_i is rewritten in the form of a linear combination of eigenvectors; $\mathbf{x}_i = \sum_k (\mathbf{x}_i \bullet \mathbf{s}_k) \mathbf{s}_k$. The projection of \mathbf{x}_i to an eigenvector \mathbf{s}_k is denoted by

$$X_k^{(i)} = \mathbf{x}_i \bullet \mathbf{s}_k, \quad (5)$$

meaning that $\mathbf{X}^{(i)} = (X_1^{(i)}, \dots, X_p^{(i)})$ represents \mathbf{x}_i in the eigenspace.

Here, an identical nano-artifact metric device can be observed in a slightly different manner depending on the observation conditions, which are affected by the misalignment or other reasons. Such fluctuations in measurements should be tolerated in order to ensure measurement stability.⁷ We quantify these fluctuations in the eigenspace as follows. Multiple measurements were performed for each of the 67 types of devices. Each measurement, for a certain identical device is denoted by \mathbf{m}_i ($i=1, \dots, K$), where K is the number of measurements. The measurement \mathbf{m}_i is represented in the eigenspace by

$$M_k^{(i)} = \mathbf{m}_i \bullet \mathbf{s}_k. \quad (6)$$

The measurement \mathbf{m}_i is represented in the eigenspace by $\mathbf{M}^{(i)} = (M_1^{(i)}, \dots, M_p^{(i)})$. Meanwhile, the N types of individual nano-artifact metrics device \mathbf{x}_i ($i=1, \dots, N$) are represented in the eigenspace by Eq. (5). The similarity between $\mathbf{M}^{(i)}$ and $\mathbf{X}^{(j)}$ is characterized by the inner product given by

$$R_{ij}^L = \sum_{k=1}^L M_k^{(i)} X_k^{(j)}, \quad (7)$$

which should be maximum when j is the designated identity that $\mathbf{M}^{(i)}$ belongs to. In Eq. (7), L denotes the number of eigenvectors considered while evaluating similarity. If L is too small, similarity does not provide an accurate classification; we quantify the minimum dimensions in identifying individual devices without errors. The ratio of inadequate classification or equivalent FNMR is evaluated for all 67 devices as a function of the dimension (L). Figure 3(a) shows six representative cases; the circular marks indicate that L should be larger than 15 to suppress the error rate to zero. Concerning all devices, the error rate results in zero, if L is larger than 38.

Furthermore, we consider the system's capacity. Let a measurement \mathbf{m}_i ($i=1, \dots, K$) or equivalently its eigenspace representation $\mathbf{M}^{(i)}$ belong to the identity j represented by \mathbf{x}_j or $\mathbf{X}^{(j)}$ in the eigenspace. The deviation of \mathbf{m}_i around the identity \mathbf{x}_j is characterized in the eigenspace by

$$\mathbf{M}^{(i)} - \left(\sum_{k=1}^L M_k^{(i)} \hat{\mathbf{X}}_k^{(j)} \right) \hat{\mathbf{X}}^{(j)}, \quad (8)$$

which represents the deviation of $\mathbf{M}^{(i)}$ from the projected vector of $\mathbf{M}^{(i)}$ on to $\hat{\mathbf{X}}^{(j)}$, as schematically shown in Fig. 3(b). Here, $\hat{\mathbf{X}}^{(j)}$ is the normalized vector of $\mathbf{X}^{(j)}$. By calculating the deviation vector given by Eq. (8) for all measurements $i=1, \dots, K$, we derive a vector representing the mean value of all measurements, denoted by $\mathbf{S} = (s_1, s_2, \dots, s_p)$, which characterizes the extent to which individual devices should span in the eigenspace while tolerating the measurement stability. Considering that the first L ($= 38$) eigenvectors are necessary to satisfy the measurement stability, the volume spanned by \mathbf{S} is characterized by the multiplication of the first L elements $\prod_{k=1}^L s_k = s_1 \times s_2 \times \dots \times s_L$. Taking the ensemble average over 67 devices, $\left\langle \prod_{k=1}^L s_k \right\rangle$ is estimated to about 8.11×10^{75} .

Meanwhile, the volume of the eigenspace spanned by different types of devices is characterized by the multiplication of the eigenvalues $\prod_{k=1}^L \lambda_k = \lambda_1 \times \lambda_2 \times \dots \times \lambda_L$,¹² which is approximately 7.29×10^{190} in the present study. Such a metric is also useful in characterizing the manipulability of robots.¹² By dividing this amount by the individual device's volume, as schematically shown in Fig. 3(c), the capacity or the number of potential identities is derived by

$\prod_{k=1}^L \lambda_k / \left\langle \prod_{k=1}^L s_k \right\rangle$, which is estimated at approximately 10^{115} or equivalently about 380 bits. This amount is significantly large, achieved by a $0.18\text{-}\mu\text{m}^2$ device indicating the huge capacity of nano-artifact metrics.

In summary, we perform eigenanalysis of the silicon nanostructures formed via resist collapse in order to clarify its potential for nano-artifact metrics. The result shows that the nanoscale morphological patterns are widely distributed in a high dimensional space; 424th order eigenvectors are needed to reconstruct 98% of the original nanostructured patterns. Considering measurement stability in the eigenspace, the estimated number of implementable different identities is approximately 10^{115} in a $0.18\text{-}\mu\text{m}^2$ nanostructure area, indicating the usefulness of nanoscale devices to accommodate huge amounts of uniqueness for future security applications. In addition, this study validates the effectiveness and the usefulness of systematic eigenanalysis methods in analyzing versatile nanostructures; the presented approach will be widely applicable to other material systems and morphological patterns on the nanometer-scale.

Acknowledgments

This work was supported in part by the Grant-in-aid in Scientific Research and the Core-to-Core Program, A. Advanced Research Networks from the Japan Society for the Promotion of Science.

References

1. H. Matsumoto and T. Matsumoto, IPSJ J. **44**, 1991 (2003).
2. R. Pappu, B. Recht, J. Taylor, and N. Gershenfeld, Science **297**, 2026 (2002).
3. D. Lim, J. W. Lee, B. Gassend, G. E. Suh, M. van Dijk, and S. Devadas, IEEE Trans. VLSI Syst. **13**, 1200 (2005).
4. J. D. Buchanan, R. P. Cowburn, A. V. Jausovec, D. Petit, P. Seem, G. Xiong, and M. T. Bryan, Nature **436**, 475 (2005).
5. M. Yamakoshi, J. Tanaka, M. Furuie, M. Hirabayashi, and T. Matsumoto, Proc. SPIE **6819**, 68190H (2008).
6. T. Ikeda, S. Hiroe, T. Yamada, T. Matsumoto, and Y. Takemura, *3rd Intl. Conf. Anti-counterfeiting, Security, and Identification in Communication 2009*, pp. 382-385.
7. T. Matsumoto, M. Hoga, Y. Ohyagi, M. Ishikawa, M. Naruse, K. Hanaki, R. Suzuki, D. Sekiguchi, N. Tate, and M. Ohtsu, Sci. Rep. **4**, 6142 (2014).
8. H. Namatsu, K. Kurihara, M. Nagase, K. Iwadate, and K. Murase, Appl. Phys. Lett. **66**, 2655 (1995).
9. R. L. van Renesse, *Optical document security* (Artech House, MA, 2004).
10. J. Gubbi, R. Buyya, S. Marusic, and M. Palaniswami, Future Generation Computer Systems **29**, 1645 (2013).
11. M. Turk and A. Pentland, Face recognition using eigenfaces, Proc. Computer Vision and Pattern Recognition 568 (1991).
12. T. Yoshikawa, *Proc. First Intl. Symposium of Robotics Research* (MIT Press, MA, 1984), pp. 735-747.
13. M. Naruse and M. Ishikawa, Appl. Opt. **39**, 293 (2000).

Figure captions

Figure 1 (a,b) The design of a resist pillars array, (a) which is collapsed randomly during the rinse process of e-beam lithography as observed in a SEM image shown in (b). (c,d) SEM images of the fabricated devices (total number: 2383) exhibiting versatile morphologies due to the random collapse. The minimum dimension is occasionally <10 nm, (c) which is considered extremely difficult to fabricate clones. Such versatilities, derived by physical randomness occurring in dimensions beyond the expected technology roadmap, are the fundamental ideas of nano-artifact metrics.⁷ (Adapted by permission from Macmillan Publishers Ltd: Scientific Reports [7], Copyright 2014)

Figure 2 Eigenanalysis of the fabricated devices. (a) Cumulative sum of the eigenvalues divided by their sum as a function of the eigenvalues' number. In retrieving 98% of the individual images, 424 eigenvectors are required, indicating that the fabricated nano-artifact metric devices span in a high dimensions in the eigenspace. (b) Examples of two-dimensional representations of the eigenvectors corresponding to the eigenvalues [from the 1st to the 10th], [from the 30th to the 39th], and [from the 400th to the 409th].

Figure 3 (a) Eigenanalysis of the measurement stability: Multiple measurements for an identical device should yield the same device identification. When the number of eigenvectors considered during identification decreases, the identification error, referred to as the false no-match rate (FNMR), increases. When more than 38 eigenvectors are considered, FNMR gives zero for all device sets. (b) System capacity estimation: considering the

deviation of each measurement from the specified identity, the total amount of deviations for multiple measurements is evaluated in the eigenspace. (c) The potential number of identities is estimated by dividing the volume of the total eigenspace by the volume of the individual devices to tolerate the measurement stability.

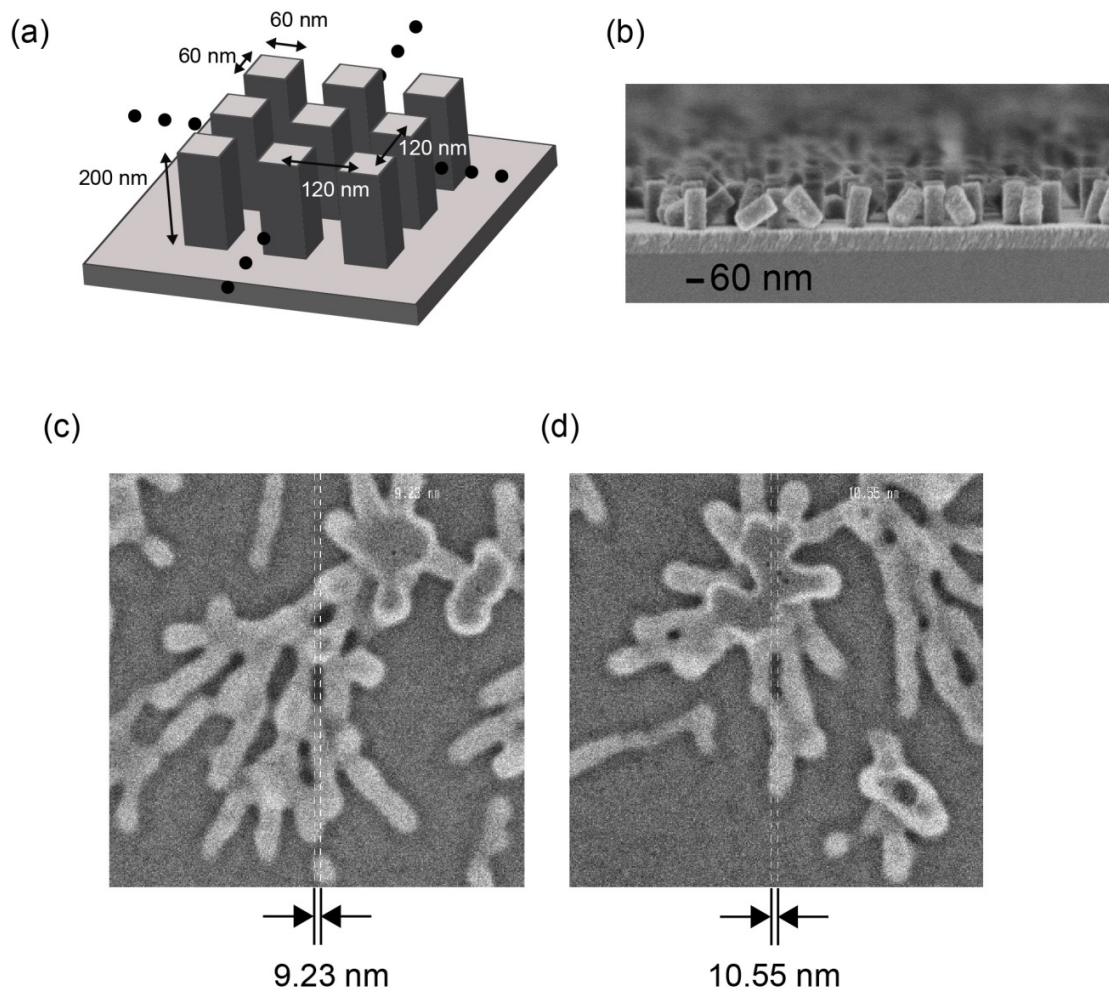


Figure 1

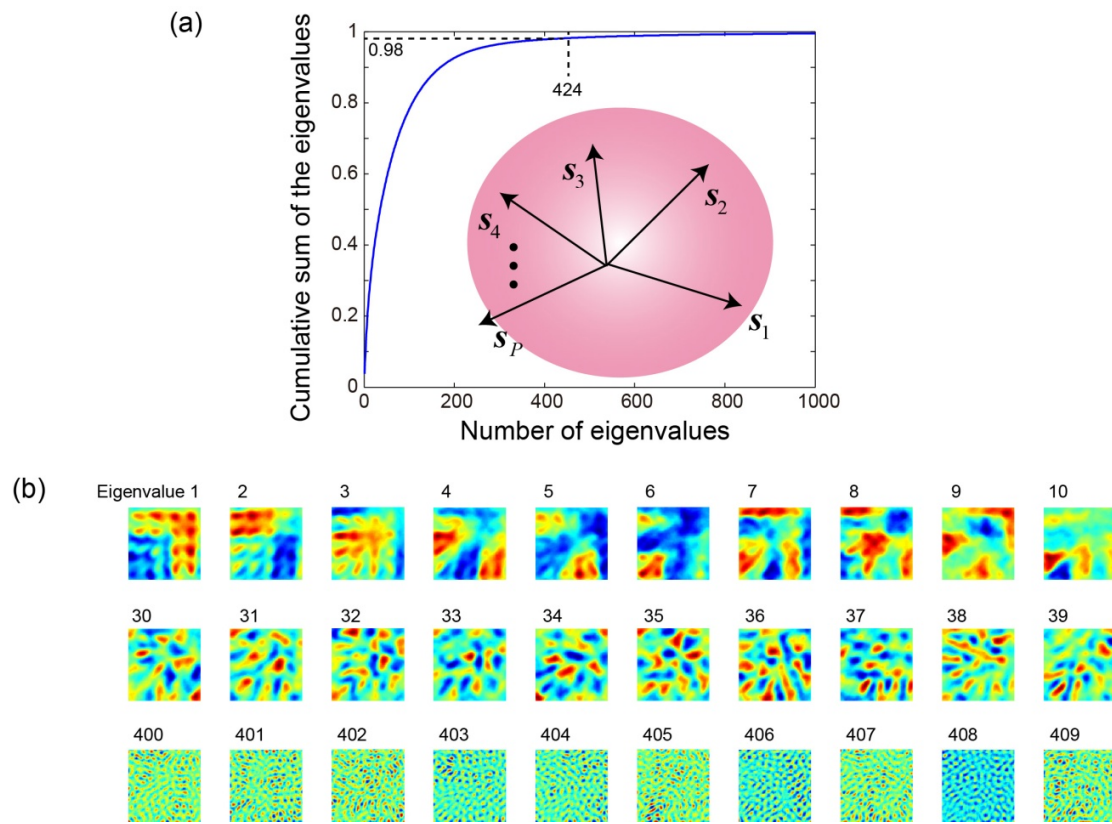


Figure 2

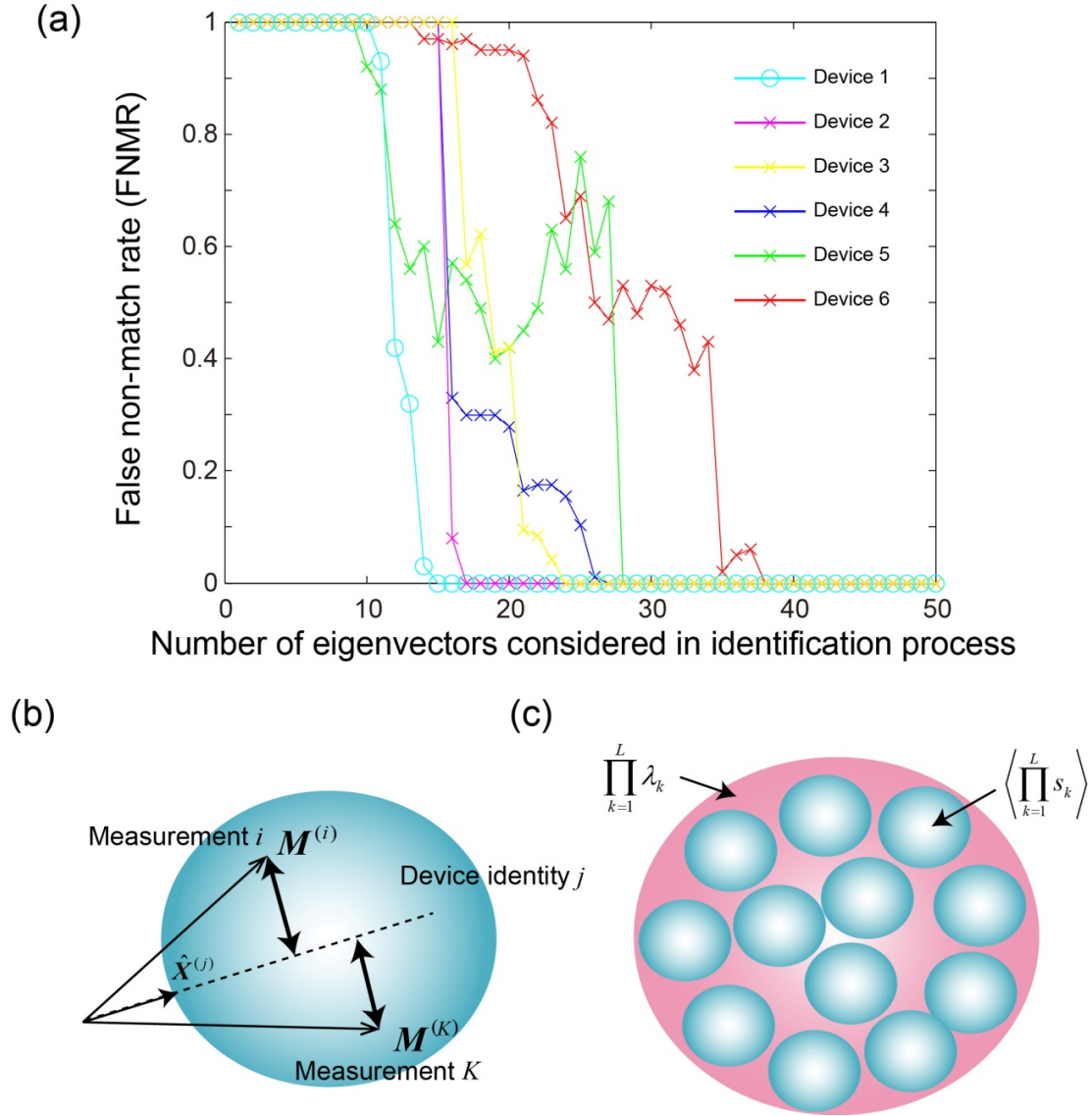


Figure 3